Rapid Communications

# Thermal-induced slippage of soft solid films

Xuanji Yu,[1,2] Fei Chen,[1,*] Chi-Hang Lam,[3] and Ophelia K. C. Tsui[1,2,4,*]

[1]*Department of Physics, Boston University, Boston, Massachusetts 02215, USA*

[2]*Division of Materials Science and Engineering, Boston University, Boston, Massachusetts 02215, USA*

[3]*Department of Applied Physics, Hong Kong Polytechnic University, Hung Hom, Hong Kong*

[4]*Department of Physics, Hong Kong University of Science and Technology, Clear Water Bay, Hong Kong*

(Received 27 March 2018; revised manuscript received 14 September 2018; published 22 January 2019)

The dynamics of interfacial slippage of entangled polystyrene (PS) films on an adsorbed layer of polydimethylsiloxane on silicon was studied from the surface capillary dynamics of the films. By using PS with different molecular weights, we observed slippage of the films in the viscoelastic liquid and rubbery solid state, respectively. Remarkably, all our data can be explained by the linear equation, $J = -M\nabla P$ and a single friction coefficient, $\xi$, where $J$ is the unit-width current, $M$ is mobility, and $P$ is Laplace pressure. For viscous films, $M$ is accountable by using conventional formulism. For rubbery films, $M$ takes on different expressions depending on whether the displacements associated with the slip velocity, $v_s(\sim\nabla P/\xi)$, dominate or elastic deformations induced by $\nabla P$ dominate. For viscoelastic liquid films, $M$ is the sum of the mobility of the films in the viscous and rubbery states.

DOI: 10.1103/PhysRevE.99.010501

Slippage is a common phenomenon [1–11]. For liquid films, it is well established. Typically, the dynamics is describable by a hydrodynamic boundary condition specified by a slip length, $b$, or equivalent friction coefficient, $\xi \equiv \eta/b$, provided $\sigma_s = \xi v_s$. (Here, $\eta$ is the viscosity of the liquid, and $v_s$ and $\sigma_s$ are the slip velocity and shear stress at the boundary, respectively [11].) However, there is no consensus on the analogous description for slipping solids. Friction measurements under low normal loads, $F_N$, [12–14] and dewetting experiments [5] revealed that $\sigma_s \sim v_s^\alpha$, with $\alpha$ varying from 0.2 to 1 [14,15]. However, at small velocities ($<\sim 0.01\ \mu$m/s), stick-slip motions ensued [12]. Friction measurements under large $F_N$'s revealed yet another set of behaviors that paralleled macroscopic friction [16]. However, these measurements usually entail damage to the substrate surface and hysteresis [13,16].

In this experiment, we studied the slippage dynamics of entangled polystyrene supported by poly(dimethyl siloxane) (PS-PDMS) by measuring the surface capillary dynamics of the films, wherein $F_N = 0$. We focused on the results obtained from the films in the rubbery state to investigate solid slippage. The dewetting phenomenon of this system had been studied in detail [5]. The results indicated that there were strong influences from the viscoelasticity of the PS film and nonlinear friction effects [15]. In those experiments, the Laplace pressure was $\sim 10^6$ Pa, comparable to the yield stress of PS [17]. The dewetting velocities were $\sim 10^{-2}$ to $\sim 10^3\ \mu$m/s [12,13,18]. Stresses and velocities of these magnitudes had been noted to cause slip transitions, and so nonlinear effects [7]. In this experiment, the Laplace pressures were tens of pascals only [19]. The flow velocity was $<\sim 10^{-8}\ \mu$m/s [19]. Under these conditions, we observed a linear relation ($\sigma_s \sim v_s$) for the films with thickness $h_0 > \sim 100$ nm in the rubbery state. For the films with $h_0 < \sim 100$ nm, the dynamics switched to one consistent with slippage amid stick-slip motions.

All polymers were purchased from Scientific Polymer Products. The weight-average molecular weights ($M_w$'s) and polydispersity indices (PDIs) of PS were 115, 393, and 940 kg/mol and <1.2, respectively. The PDMS has $M_w = 90$ kg/mol and PDI = 1.96. Silicon wafers covered by an $102 \pm 5$-nm thermal oxide were purchased from Siltronix. After cleaning by piranha solution and oxygen plasma as in Ref. [19], the substrates were coated with a PDMS film by spin coating from a toluene solution. The films were annealed at 423 K for 5 h under ~1 Pa, followed by rinsing with toluene that left the substrate with an irreversibly adsorbed PDMS layer (thickness $= 7 \pm 1$ nm). Solutions of PS in toluene were spin coated onto this layer to form PS-PDMS as in Refs. [5,18]. Film thicknesses were determined by ellipsometry and atomic force microscopy (AFM). All measurements were performed on freshly prepared PS-PDMS without aging.

Our dynamic measurement is based on the fact that as-cast spin-coated polymer films are smoother than equilibrium [19], so they roughen when heated to a sufficiently high temperature, $T$. To monitor the roughening dynamics, we captured topographic images of the sample by tapping-mode AFM after annealing it in $N_2$ for different times, $t$, at $T = 393$ K. Then the images (checked to contain no holes) were multiplied by a Welch function, Fourier transformed, and radial averaged to produce the power spectral density, PSD [19].

We had previously studied the dynamics of entangled PS on silica (PS-SiOx) by using this method [19,20]. We found that there were simultaneous fast and slow dynamic

*Corresponding authors: okctsui@ust.hk; feichen@xjtu.edu.cn

 

modes. The fast modes were attributable to the dynamics of the polymer in the rubbery state and the slow ones to those in the viscous state. To accommodate both dynamics, we used adiabatic approximation [20]. By further assuming the no-slip boundary condition, the lubrication, and linear approximations, we derived the $t$-dependent PSD [20]:

$$A_q^2(t) = A_{q,\text{short-time}}^2 \exp(2\Gamma_q t) + A_q^2(\infty)[1 - \exp(2\Gamma_q t)], \tag{1a}$$

where

$$A_{q,\text{short-time}}^2 = A_{q,0}^2 \left[\frac{3\mu_0/(h_0^3 q^2)}{\gamma q^2 + 3\mu_0/(h_0^3 q^2)}\right]^2 + A_{q,\text{elastic}}^2, \tag{1b}$$

$$\Gamma_q = -Mq^2/\{[\gamma q^2]^{-1} + [3\mu_0/(h_0^3 q^2)]^{-1}\}. \tag{1c}$$

$A_{q,\text{elastic}}^2 = k_B T/[\gamma q^2 + 3\mu_0/(h_0^3 q^2)]$ and $A_q^2(\infty) = k_B T/\gamma q^2$. Here, contributions from the van der Waals potential have been omitted as they are negligibly small (Sec. I of the Supplemental Material (SM) [21]), $\Gamma_q$ is the relaxation rate of the surface capillary wave with wave vector $q$; $k_B$ is the Boltzmann constant; $\gamma$, $\mu_0$, and $M$ denote, respectively, the surface tension, rubbery shear modulus, and mobility of the film. $A_{q,0}^2$ is the initial PSD before any annealing. $A_{q,\text{elastic}}^2$ is the PSD of a nonslipping elastic film with shear modulus $\mu_0$ and thickness $h_0$ [22]. $M$ is related to the film's viscosity, $\eta$, by $M \equiv h_0^3/(3\eta)$ [19,23]. In this model, $\tau \equiv \eta/\mu_0$ gives the onset time for the excitation of the slow modes [20,24]. Notably, Eq. (1c) is the same as that derived by Safran and Klein [25] for Maxwell liquid films with shear modulus $\mu_0$ and viscosity $\eta$, for which $\tau \equiv \eta/\mu_0$. In Eq. (1a), it is assumed that the PSD jumps from $A_{q,0}^2$ to $A_{q,\text{short-time}}^2$ in a short time (Sec. II of the SM [21]). The jump, attributable to the glass-to-rubber transition, is expected to occur in a short time ($t < 1$ s [26]) consistent with observation. After the jump, our model predicts that the PSD stays stagnant, equal to $A_{q,\text{short-time}}^2$ for $t \ll \tau$, then evolves as a liquid film with viscosity $\eta$ toward the equilibrium liquid state PSD, $A_q^2(\infty)$, when $t \gg \tau$ (dotted line in Fig. 1). Figure 1 and Fig. S2 in the SM [21] show representative sequences of PSDs we obtained (symbols) and the best fits to Eq. (1) (Secs. III and IV of the SM [21].) As one may see, the model describes the data well.

Several points are noteworthy. (i) Although residual stress should be present in our films [5,27], it did not influence the measured surface capillary dynamics [28]. (ii) The PSD of the films after the jump from the glass-to-rubbery transition or $A_{q,\text{short-time}}^2$ has two parts. One part is $A_{q,\text{elastic}}^2$, which is the PSD of the film in the rubbery state if the film had been perfectly flat from the start. From Fig. S1(b) in the SM [21], $A_{q,\text{elastic}}^2$ is truncated below a lower cutoff wave vector, $q_c = (3\mu_0/\gamma h_0^3)^{1/4}$. The second part, namely, the first term of Eq. (1b), is the low-$q$ remnant of the initial PSD after the $q > q_c$ portion of the spectrum has evolved into $A_{q,\text{elastic}}^2$ (Fig. S1(b) in the SM [21]). (iii) Equation (1) assumes the no-slip condition. If there is slippage in the films, the values of $\eta$ and $\mu_0$ obtained by fitting the data to Eq. (1) will not be the actual viscosity and shear modulus, but are effective values, denoted by $\eta_{\text{eff}}$ and $\mu_{\text{eff}}$, respectively, below. Equations (S9)–(S11) give the relations between $\mu_{\text{eff}}$ and $\mu_0$ and those between $q_c$ and $\mu_0$ under various boundary conditions (Sec. VI, SM [21]).

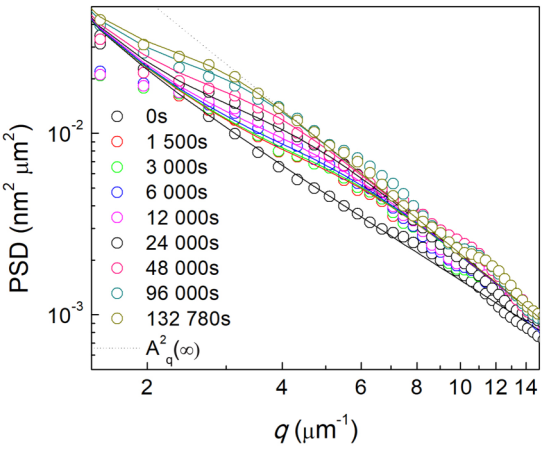


FIG. 1. A time sequence of PSDs obtained from a PS-PDMS film ($M_w = 940$ kg/mol, $h_0 = 104$ nm) with $t$ indicated in the legend. The solid lines are the best fit to Eq. (1) with $\gamma = 0.025$ N/m, $\mu_{\text{eff}} = \mu_0 = (3.4 \pm 1.0)$ kPa, and $\eta_{\text{eff}} = \eta = (1.1 \pm 0.3) \times 10^8$ Pa s. The dotted line is $A_q^2(\infty) = k_B T/\gamma q^2$.

Here, we discuss the relations between $\eta_{\text{eff}}$ (and equivalently $M$) and the physical properties of the film under different slip conditions. Consider an in-plane Laplace pressure gradient, $\partial_x P = -\gamma \partial_x^3 h(x,t)$, due to fluctuations in the film height $h_0$ along an arbitrary direction of $x$ [Fig. 2(a)]. This pressure gradient would cause a velocity profile $v(z)(//-\partial_x P)$ in the film, where $z$ is the out-of-plane coordinate. As in Refs. [19,20,22,29], we define $M \equiv -J/\partial_x P$, where $J = \int_0^{h_0} v(z)dz$ and $\eta_{\text{eff}} \equiv h_0^3/3M$. For slipping liquids, the dynamics is commonly described by the slip length, $b$ [11]. A representative velocity profile $v(z)$ of a strongly slipping liquid film (viz., $b > h_0$) is shown in Fig. 2(a). By definition, $b \equiv dv/dz|_{z=0} = v_s/b$. Assuming that the liquid viscosity is $\eta$, the shear stress at the slip boundary is $\sigma_s = \eta dv/dz|_{z=0}$. The two give the linear relation, $v_s = \sigma_s/\xi$, with $\xi \equiv \eta/b$. In the weak-slip regime [11],

$$M = h_0^3/3h + h_0^2/x \quad \text{(for slipping liquid)}. \tag{2}$$

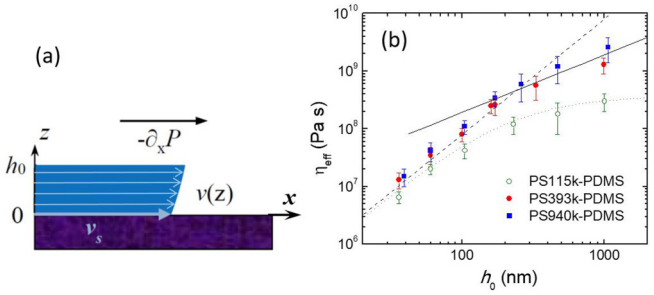


FIG. 2. (a) Experimental geometry and a representative $v(z)$ of a strongly slipping liquid due to an applied $\partial_x P$. The blue shaded area is the unit-width current, $J$. (b) Effective viscosity versus film thickness of PS-PDMS with different $M_w$'s as marked. The solid and dashed lines are the best fit to $\eta_{\text{eff}} = h_0^3/3M$, with $M = h_0^2/\xi$ and $M = h_0/(3n\tau\mu_0)$, respectively. The dotted line is a calculation using $M = h_0/(3n\tau\mu_0) + (h_0^3/3\eta + h_0^2/\xi)$.

In the strong-slip regime for overdamped dynamics, the equation of motion is [11]

$$v = (2b/\eta)\partial_x(2\eta h\partial_x v) - (bh_0/\eta)\partial_x P. \quad (3)$$

Introducing the dimensionless coordinate, $x' = x/\lambda$, where $\lambda$ is the horizontal length scale of the problem, the first term on the right-hand side can be written as $4(\beta/h_0)\partial_{x'}^2 v$, where $\beta \equiv b(h_0/\lambda)^2$ is a rescaled slip length. If $\beta/h_0 \ll 1$, which applies to our films (Sec. VII, SM [21]), this term is negligible. Equation (3) becomes $M = -J/\partial_x P = -h_0 v/\partial_x P = (bh_0^2/\eta) = h_0^2/\xi$. Clearly, this result is accountable by Eq. (2) under the presumed condition for strong slip, namely, $b \gg h_0$. Therefore, we adopt Eq. (2) for the viscous-state mobility of all our films.

In solid films, we presume that $\partial_x P$ also imparts a slip velocity, $v_s$. As before for liquid films, we propose that $v_s = \sigma_x/\xi = h_0\partial_x P/\xi$ and will verify it by experiment later. For solids, $dv/dz$ must be zero; otherwise shear strain will grow unlimitedly with time, which is unphysical. Therefore, the dynamics must be plug flow and $v(z) = v_s$. This gives $J = h_0 v_s = h_0^2\partial_x P/\xi$ and

$$M = h_0^2/x \quad \text{(for slipping solid)}. \quad (4)$$

Equation (4) implies that $\eta_{\text{eff}} = \xi h_0/3$, which is linear in $h_0$. In this work, we employ $\xi$ rather than $b$ in describing slippage because the concept of $b$ (which presumes that $dv/dz \neq 0$) is inappropriate for solids. A recent result of Cross *et al.* [14] may reflect this issue.

Figure 2(b) displays the data of $\eta_{\text{eff}}$ versus $h_0$ in a log-log scale. As one can see, the data of the PS393k and PS940k films (solid symbols) overlap. We found that $\eta_{\text{eff}} \sim h_0$ for $h_0 > 100$ nm, but $\eta_{\text{eff}} \sim h_0^2$ for $h_0 < 100$ nm. Fitting the $h_0 > 100$ nm data to Eq. (4) gives $\xi = (5.8 \pm 0.5) \times 10^6$ Pa s/nm. For the PS115k films, the data (open circles) approach a plateau value on the right, which is close to the bulk viscosity of PS115k ($\eta_{\text{bulk}} \approx 3.8 \times 10^8$ Pa s [30]). We had tried in vain to fit this data to Eq. (2). Specifically, while Eq. (2) describes the data in the plateau region well, it does poorly in the thin film region where the data converge to the $\eta_{\text{eff}} \sim h_0^2$ dependence exhibited by the higher $M_w$ films (dashed line).

To gain insight into the $\eta_{\text{eff}} \sim h_0^2$ dependence, we examine the plot of $\mu_{\text{eff}}$ versus $h_0$ [Fig. 3(a)]. There, one sees that $\mu_{\text{eff}} = 6 \pm 4$ kPa for $h_0 > \sim 100$ nm. This value agrees within a factor of ~2 with the $\mu_0$ of PS-SiOx, which is nonslipping for this range of $h_0$. [19,29]. Below ~100 nm, $\mu_{\text{eff}}$ is a function of $h_0$. Specifically, for intermediate $h_0$'s ($\sim 39 \leqslant h_0 \leqslant \sim 100$ nm), the data are describable by $\mu_{\text{eff}} = (\gamma q_{c,\text{pin}}^4/3)h_0^3$ (dashed line), where $q_{c,\text{pin}}$ is a constant with the best fit value of $4.5 \pm 0.5\,\mu\text{m}^{-1}$ provided $\gamma = 0.03$ N/m. For small $h_0$'s ($\leqslant 39$ nm), $\mu_{\text{eff}} = (16\mu_0^2/3\gamma)h_0$ using no adjustable parameters (dotted line). These observations are consistent with the substrate consisting of discrete pins separated by an average distance of $l_{\text{pin}} = 2\pi/q_{c,\text{pin}}$. For such a substrate, the capillary waves with wavelengths $2\pi/q > l_{\text{pin}}$ should see the substrate to be nonslipping (NS) [Fig. 3(b)] but those with $2\pi/q < l_{\text{pin}}$ should see it as freely slipping (FS) [Fig. 3(b)]. Concomitantly, we noted above that $\mu_{\text{eff}}(h_0)$ was consistent with the NS case (Eq. (S9) for $h_0 > \sim 100$ nm, but the FS case [Eq. (S10)] [21]) for $h_0 \leqslant 39$ nm. Then the constant $q_c$ found

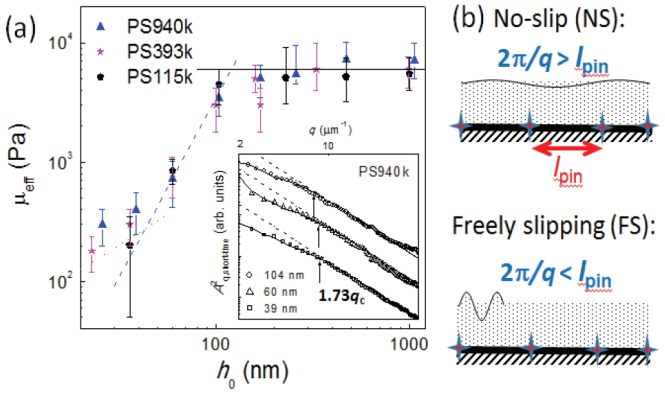


FIG. 3. (a) (Main) A summary of $\mu_{\text{eff}}$ versus $h_0$ of our films. The solid line denotes the $\mu_{\text{eff}}(h_0)$ function for NS films, namely, $\mu_{\text{eff}} = \mu_0$. The dashed line denotes that when $l_{\text{pin}} = 2\pi/q_c$ (Eq. (S11) in the SM [21]). The dotted line denotes the case when the films are FS (Eq. (S10) in the SM [21]). (Inset) Vertically shifted $A^2_{q,\text{short-time}}$ of the PS940k films with $39 \leqslant h_0 \leqslant 104$ nm showing that $q_c \approx 4.5\,\mu\text{m}^{-1}$. The dash-dot lines denote the $A_q^2(\infty)$'s. The wave vectors marked as $1.73q_c$ are where $[A_q^2(\infty) - A^2_{q,\text{elastic}}]/A_q^2(\infty) = 0.1$. (b) Drawings show why $2\pi/q_c > (<) l_{\text{pin}}$ leads to a NS (FS) case.

in the intermediate $h_0$'s [inset of Fig. 3(a)] is most naturally ascribed the value of $2\pi/l_{\text{pin}}$.

It has been noted that Eq. (4) fits the $\eta_{\text{eff}}$ versus $h_0$ data of the films with $M_w \geqslant 393$ kg/mol and $h_0 > \sim 100$ nm. But in fact, Eq. (2) does too, which is attributable to $b \gg h_0$ for these films. (By using $\eta_{\text{bulk}} = 2.1 \times 10^{10}$ Pa s for PS393k and $\xi = 5.8 \times 10^6$ Pa s/nm, one finds $b = 3700$ nm. For PS940k, $b$ is even bigger.) It is then important to clarify if our films were solid or liquid when the slow dynamics commenced. To this end, we plotted $\tau (\equiv \eta_{\text{eff}}/\mu_{\text{eff}})$ versus $h_0$ in Fig. 4. We also calculated the reptation time of the films, $\tau_{\text{rep}} (= \eta_{\text{bulk}}/\mu_0)$ by using the reported values of $\eta_{\text{bulk}}$ [29] and $\mu_0 = 6$ kPa.

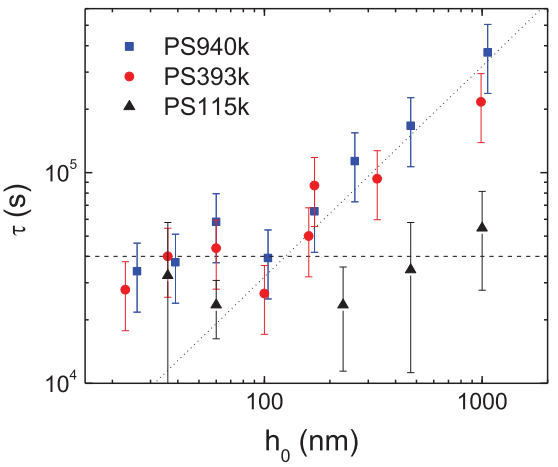


FIG. 4. Crossover time, $\tau$, for the onset of the slow-mode dynamics, plotted versus film thickness. The dotted line is the solid line in Fig. 2(b) divided by $\mu_0 = 6$ kPa. The dashed line is $\tau = 4 \times 10^4$ s, which is the average value of $\tau$ for $h_0 \leqslant 100$ nm. The error bars of $\tau$ are calculated based on propagation of uncertainties due to those of $\eta_{\text{eff}}$ and $\mu_{\text{eff}}$.

The calculation gave $\tau_{\rm rep} \approx 6 \times 10^4$ s for PS115k and $\tau_{\rm rep} \geqslant 4 \times 10^6$ for $M_{\rm w} \geqslant 393$ kg/mol. The finding, $\tau < \tau_{\rm rep}$, means that we should regard the $\eta_{\rm eff} \sim h_0$ dependence exhibited by the $M_{\rm w} \geqslant 393$ kg/mol and $h_0 > \sim$100 nm films to be a slipping solid behavior. Paradoxically, the $\mu_{\rm eff}$ of the very same films exhibited the NS character from Fig. 3(a). To reconcile these observations, we propose the substrate pins inferred from Fig. 3 to be nonpermanent and their relaxations after $\tau$ gave way to the onset of slow dynamics.

In deriving Eq. (4), it was assumed that $v_{\rm s} = \sigma_{\rm s}/\xi$. Moreover, any elastic displacements of the films due to $\sigma_{\rm s}$ were neglected. As $h_0$ decreases, $v_{\rm s}$ decreases. In addition, the elastic constant of a film, $K \sim 2\mu_0(1+\nu)h_0 \approx 3\mu_0 h_0$ (where $\nu \approx 0.5$ is Poisson's ratio) gets smaller. So at small enough $h_0$, the contribution from the film's elastic deformation to $M$ may not be ignored.

Consider a pressure gradient $\partial_x P$ acting on a solid film supported by a surface with discrete pins $\sim l_{\rm pin}$ apart. The surface stress, $\sigma_{\rm s} = -h_0 \partial_x P$ engenders pulls on the pins. Balance of forces requires that $n\langle f\rangle = h_0 \partial_x P$ where $n = 1/l_{\rm pin}^2$. When a pin (at some site $j$) is released, the forces become imbalanced. The unbalanced force $f_j$ would cause the film to slide by some amount that we label $\Delta x$. Sometime later, a new pin is formed to maintain the total number of pins equal to the same value. But generally it does not contribute to the force balance as it is most likely formed after the system has reached equilibrium. Assuming a linear response, $\Delta x \sim -f_j/K$. If $\tau_{\rm depin}$ is the lifetime of a pin, the velocity of the film arising is $v_x \sim -\langle f\rangle/(\tau_{\rm depin} K)$. Using this, $n\langle f\rangle = h_0 \partial_x P$, $M = -v_x h_0/\partial_x P$, and $K = 3\mu_0 h_0$, we obtain

$$M \sim h_0/(3n\tau_{\rm depin}\mu_0). \tag{5}$$

This gives $\eta_{\rm eff} \sim n\tau_{\rm depin}\mu_0 h_0^2$. On fitting Eq. (5) to the $M_{\rm w} \geqslant 393$ kg/mol and $h_0 < 100$ nm data, we obtain $\eta_{\rm eff} \sim 8000 h_0^2$ [dashed line, Fig. 2(b)]. To estimate the theoretical value of the prefactor, $n\tau_{\rm depin}\mu_0$, we use $n = (5 \pm 1) \times 10^{11}\,{\rm m}^{-2}$, $\tau_{\rm depin} = \tau = (4 \pm 3) \times 10^4$ s and $\mu_0 = 6$ kPa, which give 120 Pa s/nm$^2$, i.e., 67 times smaller than the experimental value. In the above derivation, we had assumed that only $h_0 \partial_x P$ and the pinning forces $f_j$ act on the film, but in practice, there could be other forces. Damman *et al.* [6] found that the PS-PDMS interfaces were diffusive. With this, the picture portrayed above, with each pin possessing the same strength, is clearly too simple. Instead, there must be numerous shorter pins that though they may not contribute to steady-state observables, such as $n$, they may contribute to $\xi$, making $\eta_{\rm eff}$ higher.

Next, we account for the $\eta_{\rm eff}$ versus $h_0$ of the 115 kg/mol films. Figure 4 shows that $\tau \sim \tau_{\rm rep} = 6 \times 10^{-4}$ s. Then the slippage dynamics of these films in the liquid state may contribute to $M$ besides those of the rubbery state. We thus write $M$ to be $M = h_0/(3n\tau\mu_0) + (h_0^3/3\eta + h_0^2/\xi)$. By using the best fit values of $1/(3n\tau\mu_0)$ and $\xi$ found above and $\eta = \eta_{\rm bulk}$ for PS115k, we attained excellent agreement with experiment without using any adjustable parameters [dotted line, Fig. 2(b)].

It is remarkable that a single value of $\xi$ is able to fit all the data. By using this value, we estimate that $b \equiv \eta/\xi = 66 \pm 13$ nm for the PS115k films. This value is comparable, within uncertainty, to that measured for PDMS on PDMS adsorbed on Si by dewetting ($\approx$250 $\pm$ 180 nm) [31] upon rescaling to match the $M_{\rm w}$ using $b \sim \eta \sim M_{\rm w}^{3.4}$. The smaller slip length we found might be due to the higher $M_{\rm w}$ of our PDMS (namely, 90 k as opposed to 8.8 k [31]). Higher $M_{\rm w}$ of the adsorbed polymer engenders a broader interface [32] and hence bigger $\xi$.

We acknowledge funding support from the Research Grant Council of Hong Kong (Awards No. 15301014, No. 16302917, No. 16303418, and No. 15330516) and the National Science Foundation (Award No. DMR-1310536).

[1] P. G. de Gennes, Rev. Mod. Phys. **57**, 827 (1985).
[2] C. Redon, F. Brochard-Wyart, and F. Rondelez, Phys. Rev. Lett. **66**, 715 (1991).
[3] Y. Zhu and S. Granick, Phys. Rev. Lett. **88**, 106102 (2002).
[4] K. Kargupta, A. Sharma, and R. Khanna, Langmuir **20**, 244 (2004).
[5] G. Reiter, M. Hamieh, P. Damman, S. Sclavons, S. Gabriele, T. Vilmin, and E. Raphael, Nat. Mater. **4**, 754 (2005).
[6] S. Coppee, S. Gabriele, A. M. Jonas, J. Jestin, and P. Damman, Soft Matter **7**, 9951 (2011).
[7] K. B. Migler, H. Hervet, and L. Leger, Phys. Rev. Lett. **70**, 287 (1993).
[8] P. P. Drda and S.-Q. Wang, Phys. Rev. Lett. **75**, 2698 (1995).
[9] F. Brochard and P. G. de Gennes, Langmuir **8**, 3033 (1992).
[10] F. Brochard Wyart, C. Gay, and P.-G. de Gennes, Macromolecules **29**, 377 (1996).
[11] O. Baumchen and K. Jacobs, J. Phys.: Condens. Matter **22**, 033102 (2010).
[12] L. Bureau and L. Leger, Langmuir **20**, 4523 (2004).
[13] A. Casoli, M. Brendle, J. Schultz, P. Auroy, and G. Reiter, Langmuir **17**, 388 (2001).
[14] B. Cross, C. Barraud, C. Picard, L. Leger, F. Restagno, and E. Charlaix, Phys. Rev. Fluids **3**, 062001(R) (2018).
[15] T. Vilmin and E. Raphael, Eur. Phys. J. E **21**, 161 (2006).
[16] B. Bhushan, J. N. Israelachvili, and U. Landman, Nature **374**, 607 (1995).
[17] G. Reiter, Phys. Rev. Lett. **87**, 186101 (2001).
[18] P. Damman, S. Gabriele, S. Coppée, S. Desprez, D. Villers, T. Vilmin, E. Raphaël, M. Hamieh, S. Al Akhrass, and G. Reiter, Phys. Rev. Lett. **99**, 036101 (2007).
[19] F. Chen, D. Peng, C.-H. Lam, and O. K. C. Tsui, Macromolecules **48**, 5034 (2015).
[20] C.-H. Lam, O. K. C. Tsui, and D. Peng, Langmuir **28**, 10217 (2012).
[21] See Supplemental Material at http://link.aps.org/supplemental/10.1103/PhysRevE.99.010501 for additional supporting data and further details about the theoretical models used in the analyses.

[22] G. H. Fredrickson, A. Ajdari, L. Leibler, and J. P. Carton, Macromolecules **25**, 2882 (1992).
[23] Z. Yang, Y. Fujii, F. K. Lee, C.-H. Lam, and O. K. C. Tsui, Science **328**, 1676 (2010).
[24] D. Peng, Z. Yang, and O. K. C. Tsui, Macromolecules **44**, 7460 (2011).
[25] S. A. Safran and J. Klein, J. Phys. II **3**, 749 (1993).
[26] A. Dhinojwala, G. K. Wong, and J. M. Torkelson, J. Chem. Phys. **100**, 6046 (1994).
[27] K. R. Thomas and U. Steiner, Soft Matter **7**, 7839 (2011).
[28] K. Geng, F. Chen, Z. Yang, and O. K. C. Tsui, in *Non-Equilibrium Phenomena in Confined Soft Matter*, edited by S. Napolitano (Springer, Basel, Switzerland, 2015), p. 25.
[29] Z. Yang, A. Clough, C.-H. Lam, and O. K. C. Tsui, Macromolecules **44**, 8294 (2011).
[30] J.-C. Majeste, J.-P. Montfort, A. Allal, and G. Marin, Rheol. Acta **37**, 486 (1998).
[31] G. Reiter and R. Khanna, Langmuir **16**, 6351 (2000).
[32] M. W. Matsen and J. M. Gardiner, J. Chem. Phys. **115**, 2794 (2001).